



A single-chain fab derived drug conjugate for HER2 specific delivery

Ruolin Xu, Yan Zheng, Wanyi Tai*

Department of Pharmaceutical Engineering, School of Pharmaceutical Sciences, Wuhan University, Wuhan, Hubei, 430071, China

ARTICLE INFO

Keywords:

scFab
Sortase A ligation
Fab-drug conjugate
SN38
His-rich linker

ABSTRACT

Despite the development of antibody-drug conjugates, the fragment Fab-based drug conjugates offer some unique capabilities in terms of safety, clearance, penetration and others. Current methods for preparing Fab drug conjugates are limited by the availability and stability of Fab proteins, leaving reports on this rare. Here, we found that a single-chain scaffold of Fab enables stabilization of the paired structure and supports high-yield expression in bacteria cytoplasm. Furthermore, we conjugated anti-neoplastic agent SN38 to the C-terminus by sortase A ligation and generated a homogenous Fab conjugate with the drug-to-Fab ratio of 1. The resulting anti-HER2 Fab-SN38 conjugate demonstrated potent and antigen-dependent cell-killing ability with the aid of its special cathepsin-triggered cyclization-promoted release mechanism. In vivo, Fab-SN38 can prevent growths of HER2-positive tumors in athymic mice and be well tolerated to the treatment at 7 mg/kg per dose. Anti-tumor activity, high dose tolerance and penetration advantage observed in this study would merit Fab conjugate investigation in target chemotherapy.

1. Introduction

Antibody-drug conjugate (ADC) is an emerging class of therapeutic agents that enables the selective delivery of cytotoxic payloads to tumors via monoclonal antibodies (mAb) [1]. It combines the advantages of target specificity, potent killing effect and long circulation half-life to achieve an efficient elimination of cancer cells [2]. To date, 13 ADCs have gained approvals from the U.S. Food and Drug Administration (FDA), and over 100 are evaluated in clinical trials encompassing a broad variety of cancer types [3]. Despite considerable success in clinics, the potential of ADC in cancer treatment is often limited by various factors [4]. For example, the payloads of ADCs are highly toxic and exhibit very narrow therapeutic windows [5]; their non-specific exposure to off-target tissues may cause unacceptable side effects [6]. Additionally, the high molecular weight of ADC (~150 kDa) also poses problems like poor tumor penetration, long systemic exposure, slow clearance and Fc-mediated side effects [7–9]. Indeed, many ADCs have been withdrawn either from the market or clinical trials owing to their severe toxicity and low therapeutic index [10]. Safety-related issues of ADC have been extensively reported and discussed in many literatures [11–14].

Some innovative molecular designs have been proposed to tackle these clinical challenges [10]. In particular, the antibody fragment-derived drug conjugates, such as Fab-drug conjugate, offer

some unique capabilities [15]. Compared to the whole antibody, Fab might be an ideal format as a drug carrier, because it not only has a faster clearance and better tumor-to-blood ratio than full-length antibody but also exhibits a higher stability and better targeting capability than other fragments, i.e. scFv [16]. This fragment discards the Fc domain, thus would avoid the Fc-mediated toxicities such as dose-limiting thrombocytopenia reported with trastuzumab emtansine (T-DM1) [8]. A shorter systemic exposure and less effector-mediated toxicities of Fab also open a possibility to utilize less potent but more tolerable payloads such as paclitaxel, vinblastine, SN38, et, al., that allows escalating the dosage and administration frequency [17,18].

In spite of the interest, the reports on Fab-drug conjugates remain rare. One obstacle to its application is the Fab availability [19]. A straightforward preparation of Fab is via papain digestion of full-length antibodies [20,21], but owing to cost reasons it has been replaced by the recombinant technology [22]. However, like many other cysteine-rich proteins, the recombinant Fab is classically expressed in the *E. coli* periplasm [23]. The bacterial periplasm offers a desired environment for proper folding and disulfide oxidation [24], but Fab expression in this route generally gives a minimal protein product yield (<1 mg/L) due to the narrow compartment space [25,26]. Moreover, the correct pairing of light and heavy chains by disulfide bond is also a challenge during Fab production. The inefficient formation of disulfide bond has been reported in many Fab expression experiments, including *E. coli*, *Pichia*

* Corresponding author.

E-mail address: wanyi-tai@whu.edu.cn (W. Tai).

<https://doi.org/10.1016/j.biomaterials.2024.122798>

Received 10 March 2024; Received in revised form 19 August 2024; Accepted 31 August 2024

Available online 2 September 2024

0142-9612/© 2024 Elsevier Ltd. All rights are reserved, including those for text and data mining, AI training, and similar technologies.

pastoris and insect cell expression systems [26–30]. Some effort has been directed toward amino acid mutations on the constant regions (light constant and constant heavy-1) to enhance assembly between light and heavy chains of Fab [31]. Therefore, massive production of Fab is one of the challenges in front of Fab-drug conjugate development.

In this study, a high-quality Fab, produced in a single-chain format from bacteria, was conjugated with SN38 and evaluated for human epidermal growth factor receptor 2 (HER2) specific chemotherapy. The single-chain Fab (scFab) has been previously adapted as a Fab alternative for phage display [32]. Here we found that this scaffold can be

efficiently expressed in bacterial cytoplasm with the aid of an optimized 63aa polypeptide linker (his-rich loop). In solution, it exists predominantly as monomers and correct light/heavy chain pairs owing to the proximity effect of the single chain. After the TEV cleavage and sortase A ligation, this anti-HER2 Fab was successfully conjugated with antineoplastic agent SN38 via a special VCit linker, that can promote a traceless payload release by a cathepsin-triggered ring closure reaction. In vitro and in vivo evaluation of Fab-SN38 conjugate demonstrated its high specificity to HER2-positive cells as well as a promising therapeutic effect in athymic mice. This technique may be applied to develop the drug

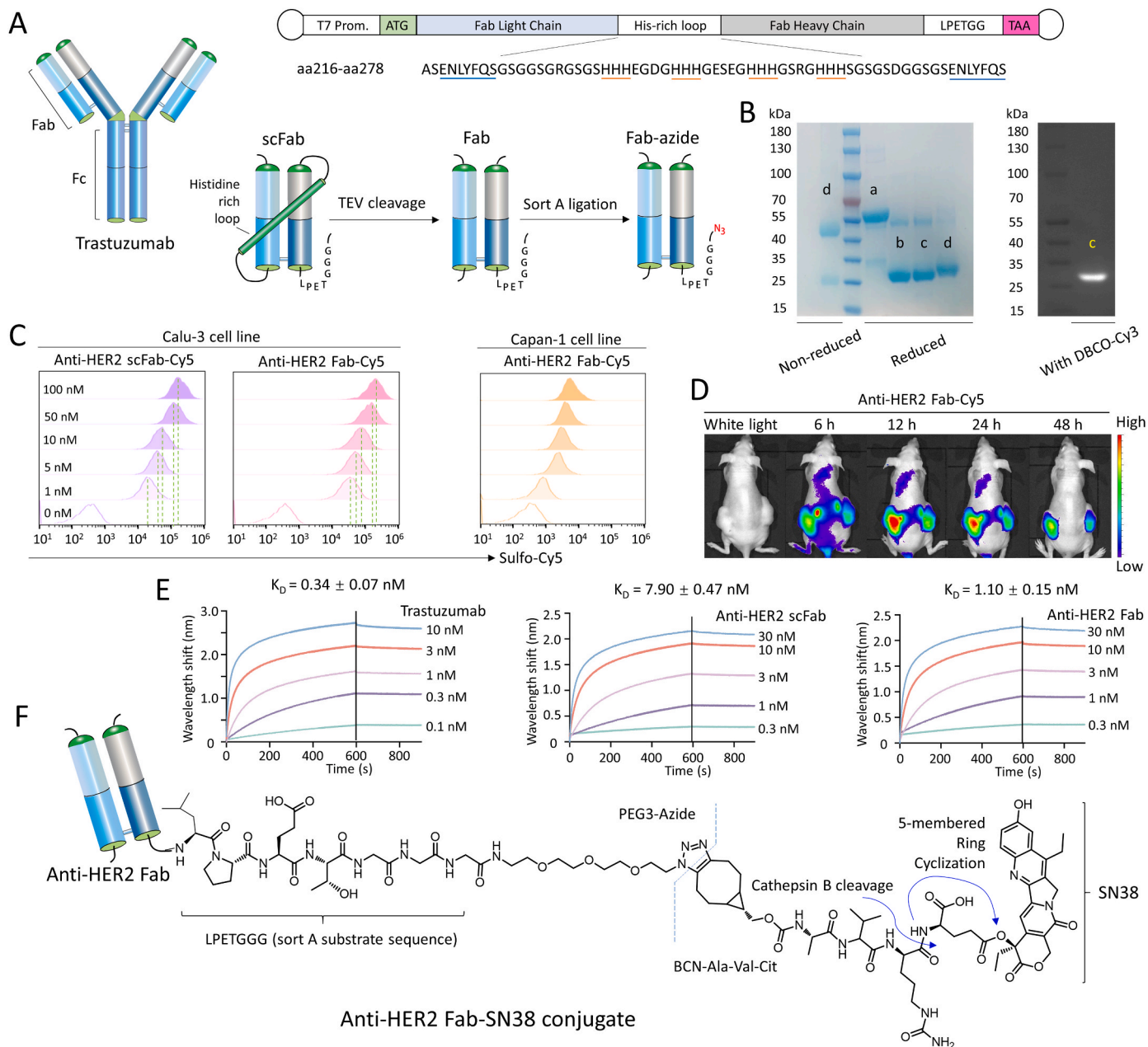


Fig. 1. The scheme of the anti-HER2 Fab-SN38 conjugate. (A) An anti-HER2 Fab was derived from mAb trastuzumab. A scFab scaffold was constructed by linking the C-terminus of light chain to the N-terminus of heavy chain with a histidine rich loop (aa216-aa278). The scFab was converted back into Fab by TEV processing, followed by ligating an azide group at the C-terminus via the sortase A mediated transpeptidation. The gene expressing cassette of scFab was depicted above. The his-rich loop contains two ENLYFQS (blue underline) epitopes at the sides of loop for TEV cleavage and four histidine clusters (yellow underline) in the middle for the Ni-NTA purification of scFab. (B) SDS-PAGE characterization of the corresponding protein variants. Lane a, scFab; lane b, Fab; lane c, Fab-azide; lane d, Fab-SN38. The presence of azide group in lane c was confirmed by DBCO-Cy3 (copper-free click chemistry). (C) The binding of scFab and Fab to HER2-positive Calu-3 and Capan-1 cells. (D) A comparison of the Fab targeting capacity between Calu-3 tumor (left dorsal) and Capan-1 tumor (right dorsal) in one mouse. (E) Quantitative analysis of K_D values using BLI. (F) The structural illustration of the anti-HER2 Fab-SN38 conjugate. (For interpretation of the references to color in this figure legend, the reader is referred to the Web version of this article.)

conjugates of other Fabs.

2. Results

2.1. The scFab construct and its conversion to Fab

In an effort to obtain the correctly paired Fab, we introduced a scFab design (Fig. 1A). In this scaffold, the C-terminus of the light chain (LC) is fused to the N-terminus of the heavy chain (HC) via a flexible His-rich loop. This 63-amino-acid loop (aa216-aa278) contains large numbers of glycine and serine (GS) to ensure the flexibility, and it also covers a linear distance of ~ 145 Å to mitigate the steric strain during the folding of Fab domains. Four histidine clusters (His \times 3) and 2 TEV substrate epitopes were spatially inserted among the loop to allow the scFab purification and TEV protease-mediated loop removal. Furthermore, the proximity effect of the single chain helps retain the disulfide bond (indicated by a green stick in Fig. 1A) that connects the C-termini of LC and HC, with an assumption of better stability and productivity in bacteria.

The scFab protein was expressed in *E. coli* and then purified using Ni-affinity chromatography with a yield over 100 mg/L. Subsequently, the his-rich loop was chopped off by the TEV protease (Fig. S1), which not only unfolds the native Fab structure but also eradicates the potential immune risk from the exogenous loop sequence. The conversion of scFab to Fab achieved a high efficiency, with almost complete removal of the his-rich loop and an overall yield of approximately 75% after ion exchange purification. Surprisingly, the SDS-PAGE image in Fig. 1B showed that the single-chain scFab (54.530 kDa) was cleaved into a smaller one but not two bands once treated with TEV protease. This band was likely mingled with both Fab LC and HC chains due to their molecular weight similarity (24.527 kDa and 24.635 kDa, respectively). It was gratifying to note that the linker removal had not come at the expense of physical stability as commonly seen in most scFv (Fig. S2). Instead, it helps to regain some degree of HER2 binding capacity as shown in Fig. 1C. Both Calu-3 (HER2 high expression) and Capan-1 (HER2 low expression) can be well recognized by this anti-HER2 Fab, even at a concentration as low as 1 nM (Fig. 1C). We further investigated the targetability of the Fab protein to subcutaneous xenografts. The sulfo-Cy5 labeled Fab was administered to the mice bearing both Calu-3 (left dorsal) and Capan-1 (right dorsal) tumors. The *in vivo* distribution results showed that the Fab-Cy5 was specifically accumulated at both tumor sites, but exhibited a higher deposition in Calu-3 tumor, which was a reflection of its HER2 expression status (Fig. 1D). To quantitatively evaluate the binding capability, the dissociation constant (K_D) of Fab to HER2 receptor was measured, and compared with trastuzumab and scFab using the biolayer interferometry (BLI) (Fig. 1E). It is noted that the Fab ($K_D = 1.10 \pm 0.15$ nM) exhibits a much higher binding affinity to HER2 than scFab ($K_D = 7.90 \pm 0.47$ nM), although it remains weaker than the full-length antibody trastuzumab ($K_D = 0.34 \pm 0.07$ nM). The compromise of affinity in scFab is likely ascribed to the wrapping effect of his-rich loop, indicating the necessity of linker removal. These experimental results demonstrate the good targeting and binding ability of scFab derived Fab.

2.2. Drug conjugation to anti-HER2 Fab

To achieve site-specific conjugation with the payload SN38, the C-terminus of the scFab protein was genetically coded with a sortase A substrate peptide sequence (LPETGG) for sortase A manipulation. Briefly, the Fab protein was dissolved in TBS buffer and then co-incubated with GGG-PEG3-azide in the presence of sortase A overnight (Fig. S3). This step allows a ligation of the carboxyl terminus with an azide for later click drug conjugation. The turnover of this ligation cannot be distinguished by SDS-PAGE because of the tiny molecular weight gain in the product, but confirmed by co-incubating the purified Fab-azide with the fluorescent dye DBCO-Cy3. The Cy3 fluorescence of

its band in Fig. 1B indicated the presence of azide groups in products, a reflection of the successful transpeptidation.

Next, we set out to synthesize a bicyclononyne (BCN) functionalized linker-drug conjugate BCN-VCit-SN38 for copper-free conjugation with Fab-azide. As the structure depicted in Fig. 1F, the payload SN38 was connected to the VCit linker through a glutamic ester bond. Upon internalization by target cancer cells, we expected that the VCit linker would be cleaved by cathepsins in endosomes, which leads to the 5-member ring closure reaction and a traceless release of SN38. BCN-VCit-SN38 was synthesized according to the synthetic route in Scheme 1. The product was characterized by high-resolution mass spectrometry and high-performance liquid chromatography (HPLC) to confirm the molar mass and purity (Fig. S4).

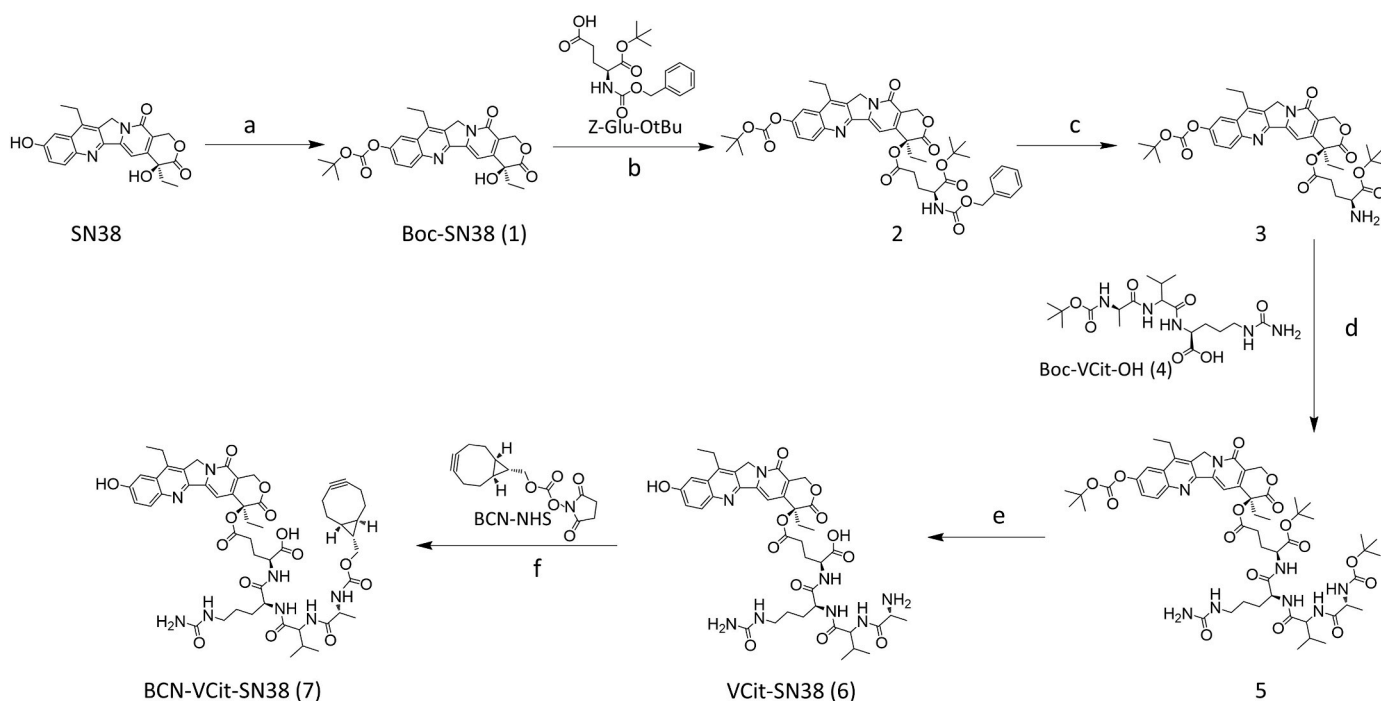
Subsequently, BCN-VCit-SN38 was reacted with the Fab-azide using copper-free click chemistry. The excess linker-drug was removed by the size exclusion chromatography (Fig. S5) and the obtained conjugate Fab-SN38 was resolved on SDS-PAGE gel in either reduced or non-reduced condition (Fig. 1B). The reduced SDS-PAGE gel revealed two adjacent bands, which can be assigned to the Fab LC and HC, respectively. This observation is consistent with the calculation that the drug appended HC (25.536 kDa) is around 1kDa larger than the LC (24.527 kDa). Under non-reduced conditions, a single band was observed in the range between 55 kDa and 40 kDa, in agreement with the calculated molecular weight of 50.061 kDa, which is suggestive of the successful drug conjugation.

2.3. Cathepsin B promoted tandem release of payloads

To investigate whether SN38 can be released in its free form, we first evaluated VCit-SN38 for cathepsin B-mediated cleavage. Cathepsin B is a key lysosomal protease that plays a crucial role in the regulation of physiological and pathological processes. It has been demonstrated that aberrant overexpression of cathepsin B is associated with the progression of oncogenic activation [33]. The conjugate was incubated in the presence of bovine spleen cathepsin B in a sodium acetate/EDTA/DTT buffer (pH 5.5) at 37 °C. The samples were then analyzed by HPLC at the indicated time points to monitor the consumption. The HPLC tracing in Fig. 2A illustrates a gradual decrease in the peak area of VCit-SN38 over time, accompanied by a gradual increase in the Glu(SN38)-OH peak. All the fragments in the reaction were verified by high-resolution mass spectrometry. Surprisingly, no free SN38 was released in this proteolytic reaction, even with an extension of incubation time overnight. We speculated that the ring-closing metathesis of Glu(SN38)-OH cannot occur at acidic pH, because the alpha amine of Glu is protonated and unable to trigger the nucleophilic attack. When the pH rose to 7.4, the release of SN38 was observed in the HPLC spectra (Fig. 2B and C). The SN38 peaks rose in concomitant with the peak decrease of Glu(SN38)-OH, which eventually disappeared after 20 h.

The releasability of SN38 raises a concern about the stability of the ester bond between SN38 and γ -carboxyl of Glu. Most ester bonds are readily attacked by ubiquitous esterases in serum and exhibit the half-life of only a couple hours. It is fortunate that the ester at the 20-hydroxy position of SN38 is well-known for its resistance to hydrolysis own to the high steric hindrance. This proof of concept has been demonstrated by the FDA-approved ADC sacituzumab govitecan which conjugates SN38 at this position using a carbonate ester and exhibits a serum half-life over 24 h [34,35]. To confirm this assumption, we evaluated the stability of the SN38 conjugate in three different media: PBS, mouse plasma and cell culture media (RPMI 1640 supplemented with 10% FBS), respectively. The results in Fig. 2D and Fig. S6 revealed that the ester linkage is quite stable and the conjugate sustains more than 12 h in all three conditions.

Based on the data above, we speculated that the Fab-SN38 conjugate is likely processed by cathepsins in the acidic endosomal compartment to release the Glu(SN38)-OH. However, this intermediate has to diffuse into the cytosol which has a higher pH, to trigger the ring closure reaction and free the SN38 payload. The *ex-situ* release of drugs raised our



Scheme 1. Synthesis route of the BCN-VCit-SN38. Reagents and conditions: (a) $(\text{Boc})_2\text{O}$, pyridine, DCM, RT, 1.5 h; (b) Z-Glu-OtBu, EDCI, DMAP, DCM, RT, 16 h; (c) Pd/C, ethyl acetate, H_2 , RT, 4 h; (d) HATU, DIPEA, DMF/DCM (1/1), RT, 2h; (e) 40% TFA/DCM, 1 h; (f) BCN-NHS, Et_3N , DMF, RT, 2 h.

curiosity about the membrane permeability of Glu(SN38)-OH as it may affect the tandem release efficiency. To address this question, we applied Glu(SN38)-OH to the SN38-sensitive tumor cells and found that it can elicit the cytotoxic effect almost as well as SN38 (Fig. 2E). In contrast, the effect is less prominent in the group treated by Glu-SN38, which is an analog of Glu(SN38)-OH but unable to undergo the cyclization. Collectively, these results demonstrated that Glu(SN38)-OH is membrane permeable and it elicits its cytotoxic activity by releasing the potent SN38 rather than by itself because the modification at the 20-hydroxy position of SN38 (Glu-SN38) compromises its potency.

2.4. The potency to tumor cells in vitro

Cytotoxicity study reveals that the potency of SN38 ranges from 3 to 13 nM in 3 of the 4 cell lines we tested, with NCI-N87 having the lowest sensitivity of 70 nM. The in vitro bioactivity of Fab protein was also provided in Fig. 3A. In HER2-positive cells, treatment with anti-HER2 Fab disrupted HER2 signaling, leading to the growth inhibition of NCI-N87 cells by ~ 50%. MDA-MB-231, a breast cancer cell line without HER2 expression, was less affected. This trend of sensitivity observed in the Fab is similar to that of trastuzumab. However, cells' sensitivity to Fab was not always correlated with HER2 status, as the cell line Calu-3 and SK-OV-3 with high HER2 expression level were growth inhibited in a similar degree to MDA-MB-231 (15%, 17% and 3%, respectively). Nevertheless, we observed an additive effect on all HER2-positive cell lines after the treatment with Fab-SN38 conjugate (Fig. 3B). On contrast, MDA-MB-231 gives no response to the Fab-SN38 treatment, even though this cell line is most sensitive to SN38 ($\text{IC}_{50} \sim 3$ nM). Altogether, these data demonstrated that the Fab-SN38 is a potent and selective cell killer to the HER2-positive cells.

Both anti-HER2 Fab and SN38 are therapeutic agents against the HER2-positive tumor cells. Once covalently conjugated, it demonstrated an additive effect on the growth inhibition of tumor cells. For example, SN38 treatment (10 nM) induced the apoptosis of Calu-3, NCI-N87 and SK-OV-3 by around 33.5%, 29.9% and 32.6%, respectively; in contrast, 45% – 58% population of apoptosis was detected in all three cell lines treated by Fab-SN38 (Fig. 4A). The augment of potency is likely ascribed

to the addition of targeting capability but not anti-tumor activity by anti-HER2 Fab, because the Fab itself did not induce cellular apoptosis in our study. It is interesting that both anti-HER2 Fab and trastuzumab treatment can inhibit the proliferation of NCI-N87 cells by around 50%, as shown in Fig. 3A. A further analysis by flow cytometry revealed that anti-HER2 Fab arrested the NCI-N87 cell cycle at G0/G1 phase, which would impair the growth but not lead to apoptosis (Fig. 4B). In Calu-3 and SK-OV-3 cells, surprisingly Fab did not produce apparent effect on cell cycles. But Fab-SN38, as well as its payload SN38, can significantly induce cell cycle arrest in the G2/M phase in all three cell lines, suggesting increased apoptosis through DNA damage. SN38 is a camptothecin derivative that exhibits anticancer activity by selectively inhibiting the activity of topoisomerase I, an enzyme essential for DNA replication [36]. In cells, it selectively suppresses DNA replication during the S phase, arrests cells in the G2/M phase, and induces chromosomal DNA fragmentation. Our data suggest that the payload SN38 plays an indispensable role in anti-tumor activity, especially in trastuzumab-insensitive cell lines.

2.5. Binding and internalization of Fab conjugate

To further confirm the specificity to the target tumor cells, the anti-HER2 Fab-SN38 was labeled with fluorescent dye sulfo-Cy5. The cell binding and intracellular tracking experiments were performed using flow cytometry and confocal microscopy, respectively. The results in Fig. 3C demonstrate that Fab-SN38 was well bound to all the HER2-positive cells (Calu-3, SK-OV-3, Capan-1 and NCI-N87 cell lines), and the fluorescence intensity of the treated cell population shifted in correlation with the HER2 expression status (Fig. 3D) as well as the dose applied (Fig. S7). Because SN38 itself has fluorescence ($\text{ex/em} = 377/556$ nm), we can directly track the payload during receptor binding, internalization and distribution in cells by confocal microscopy. As shown in Fig. 3E, anti-HER2 Fab-SN38 can recognize the HER2 receptors of SK-OV-3 cells after 30-min coincubation at 4 °C. Because of the low temperature, the conjugates bind with the HER2 receptors, but did not trigger the receptor-binding mediated internalization, which allows us to capture a moment of both SN38 (blue) and Fab (red) colocalizing on

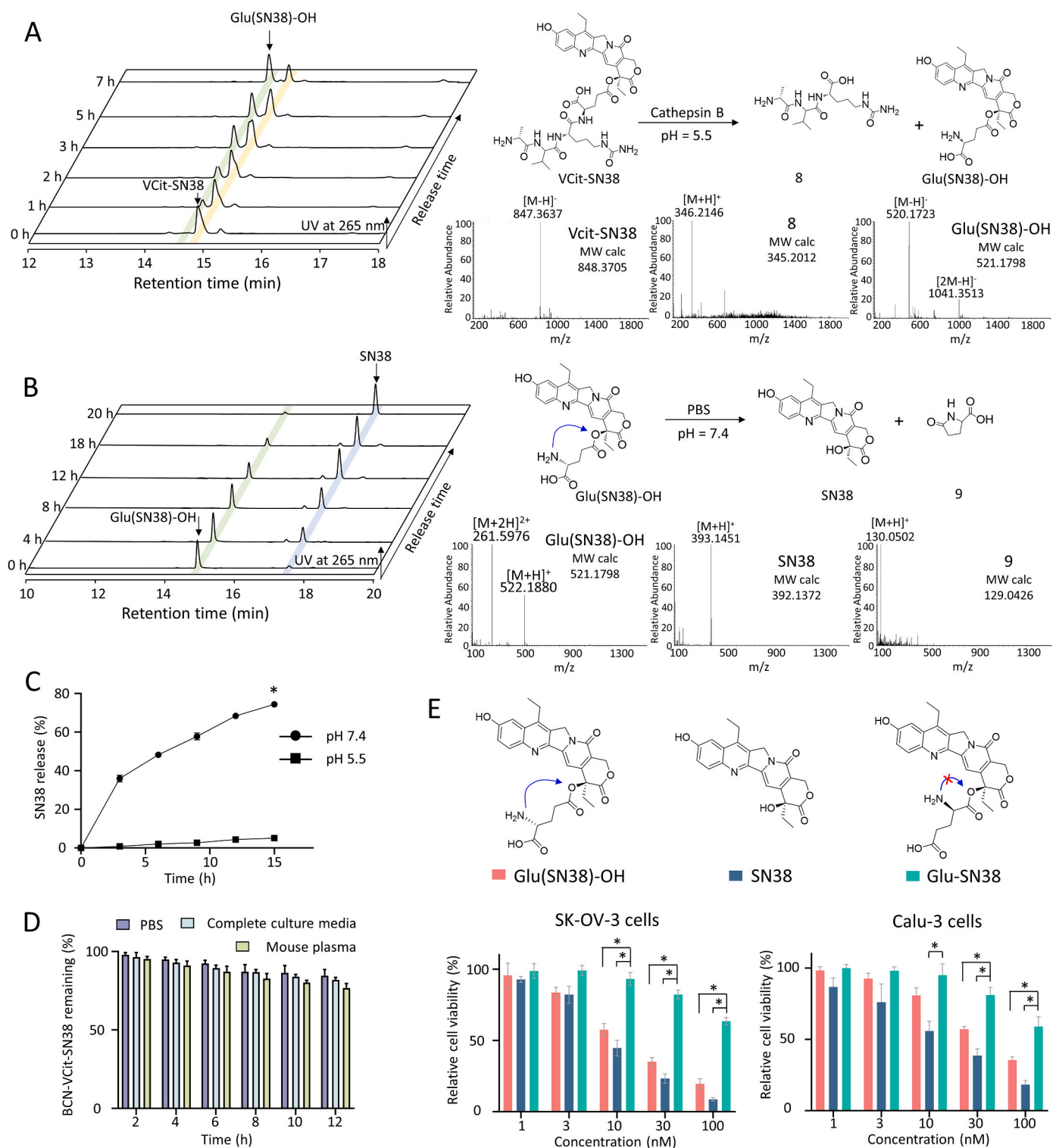


Fig. 2. In vitro SN38 release after cathepsin B cleavage and the ring closure reaction. (A) The release Glu(SN38)–OH after cathepsin B treatment at pH 5.5 and 37 °C. The reaction scheme (right above) and corresponding mass spectra (right below) were shown on the right. (B) HPLC tracing of the SN38 release from Glu(SN38)–OH in PBS buffer at 37 °C. At the neutral condition (pH 7.4), the unprotonated amino group of Glu(SN38)–OH triggers a ring closure reaction and release the SN38 (right above). The corresponding mass spectra of compounds in the reaction were shown on the right below. (C) The kinetic curves of SN38 release from Glu(SN38)–OH over time in buffers of pH 7.4 or pH 5.5 at 37 °C. Each time point was shown as mean \pm SD ($n = 3$). * $P < 0.05$. (D) The stability of the BCN-VCit-SN38 was evaluated in PBS solution, complete culture media (10% FBS) and mouse plasma, respectively. Each time point was shown as mean \pm SD ($n = 3$). (E) Cytotoxicity comparison of SN38, Glu(SN38)–OH and Glu-SN38. Data was shown as mean \pm SD ($n = 3$), * $P < 0.05$.

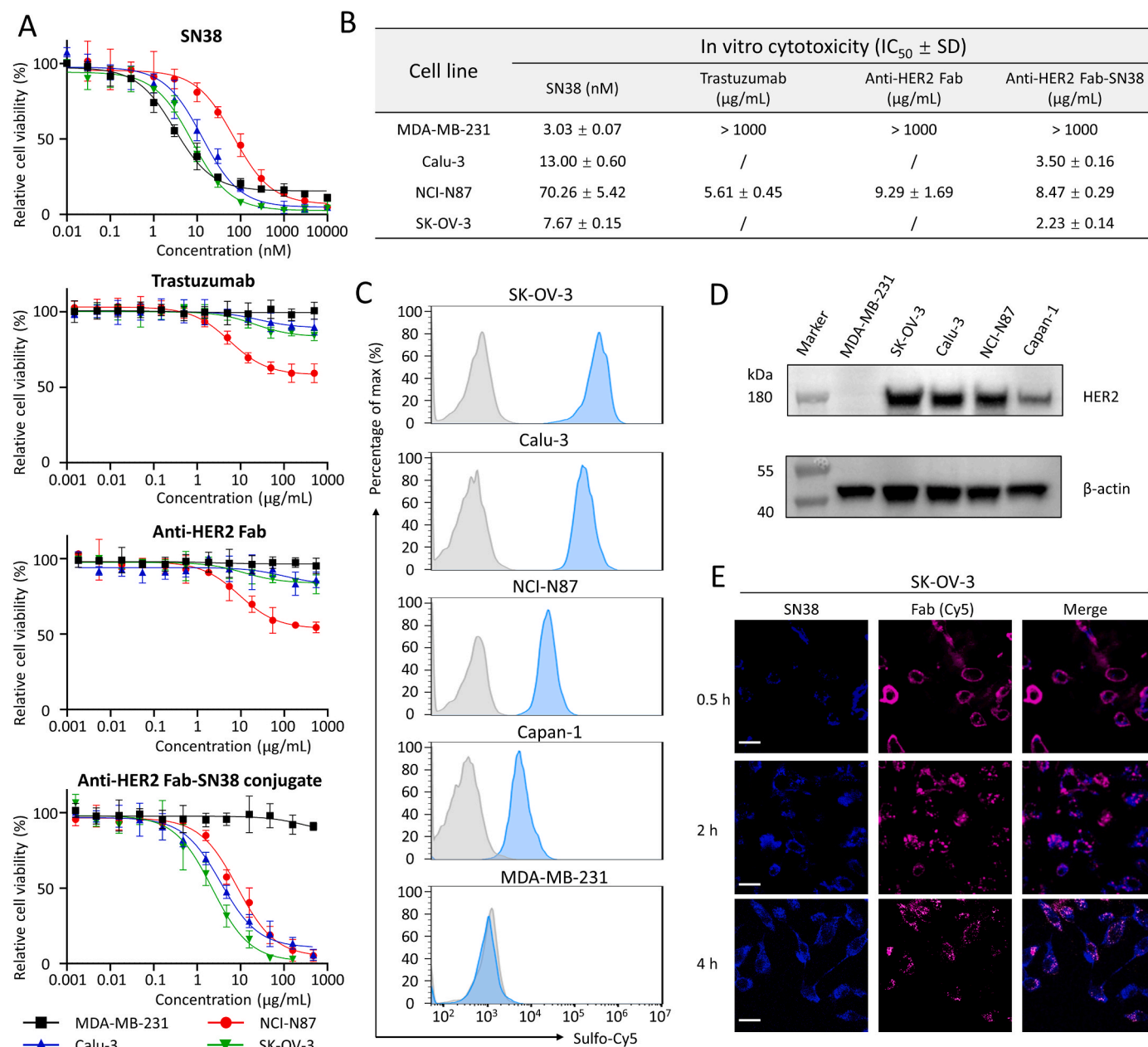


Fig. 3. The selectivity and potency of Fab-SN38 toward HER2 positive cells. (A) Viability profiling of SN38, trastuzumab, anti-HER2 Fab and Fab-SN38 on 4 cancer cell lines. The data points in the graph were shown as mean \pm SD ($n = 3$). (B) IC_{50} values from the viability assays of Fig. 3A. (C) The binding selectivity of Fab-SN38 (Cy5 labeled) to cancer cells of different HER2 status. Fab-SN38 (100 nM) was incubated with cells at RT for 1 h. The fluorescent intensity of treated cells (light blue histogram) was analyzed in comparison to untreated blank cells (grey histogram) by flow cytometry. (D) Western blotting analysis of HER2 expression level in different cell types. Beta actin was chosen as the loading control. (E) Confocal imaging of the Fab-SN38 internalization and distribution in SK-OV-3 cells. SN38 was tracked by scanning the fluorescent signal emitted by itself. Scar bar, 25 μm . (For interpretation of the references to color in this figure legend, the reader is referred to the Web version of this article.)

the cell membrane. With an increase in temperature and time, internalization occurred. The overlap of SN38 and Cy5 fluorescence was observed in both the cell boundary and cytoplasm, indicating that Fab-SN38 had entered the cells via receptor-mediated internalization. It is aware that a significant amount of SN38 (blue) diffused into the cytoplasm at 4 h, in contrast to the restriction of Fab (Cy5) in membrane and endosomes only, which may be attributed to the proteolysis of the VCit linker by cathepsins and the concomitant release of SN38.

2.6. In vivo imaging in solid tumor xenografts

The promising results in vitro prompted us to investigate the

conjugate's performance in vivo. Fab-SN38 was labeled with sulfo-Cy5 and injected into the NCI-N87 tumor-bearing mice via the tail vein. As the near-infrared (NIR) imaging shown in Fig. 5A, drug accumulation in tumors was observed 6 h after injection, and the intense fluorescence persisted in NCI-N87 tumors for at least 48 h. In contrast, the fluorescence in mice injected with sulfo-Cy5 labeled VCit-SN38 (without targeting ligand) decayed rapidly, with fluorescence nearly undetectable in the tumor by 48 h. In comparison to Fab, the sulfo-Cy5 labeled trastuzumab demonstrated a similar strength of accumulation and persistence in tumors. However, it exhibits a much broader distribution in mouse bodies than the Fab-SN38 conjugate, especially at 6 h and 12 h post administration, indicating a slower systemic clearance. This observation

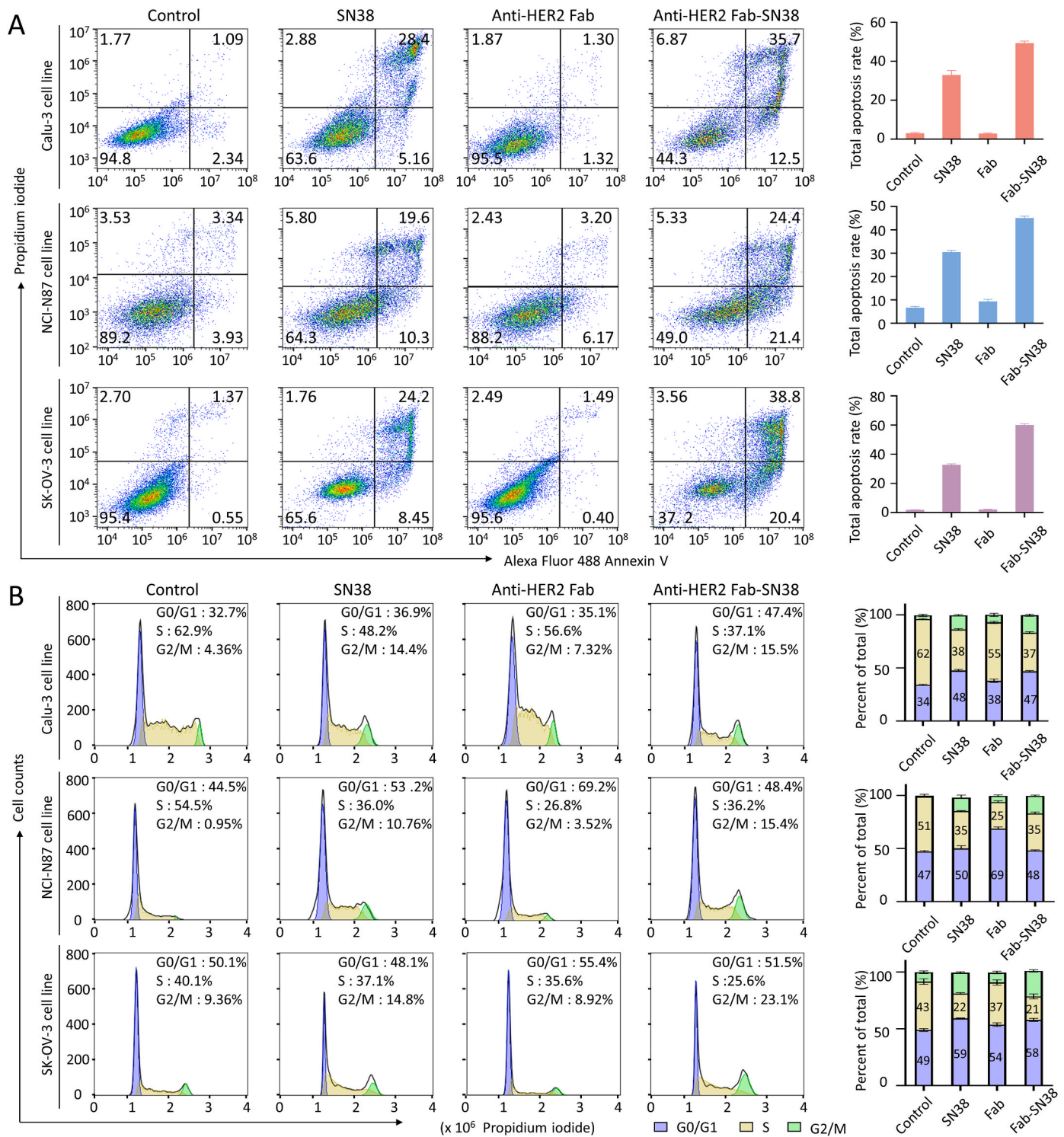


Fig. 4. Cell health assay after the treatment by SN38 (10 nM), anti-HER2 Fab (10 µg/mL) and Fab-SN38 conjugate (10 µg/mL). (A) Scatter charts of the viable cells (bottom left), early apoptosis (bottom right), late apoptosis (top right) and necrosis (top left) were measured by flow cytometry in HER2-positive cells after exposure for 36 h to PBS (control) or drugs. All the groups were repeated in triplicate and the apoptotic rates were compared as mean ± SD in right. (B) Flow cytometry to evaluate cell cycle after 24-h treatment by either PBS (control) or drugs. The numerals in the boxes of right panels represent the average proportion of cells in each cycle of three independent experiments.

was further confirmed by NIR imaging of the dissected organs and tumors in Fig. 5B. Fab-SN38 showed minimal accumulation in the heart, liver, lung and spleen, but was predominantly visible in the tumor. Trastuzumab, on the other hand, showed a high deposition in the liver along with the tumor. Both Fab-SN38 and VCit-SN38 were detected in the excretory organ kidney, but not the liver, indicating their

elimination via the urinary system (Fig. 5C and D).

The enhanced deposition in the tumor is likely ascribed to the improvement of pharmacokinetics by Fab conjugation in comparison to the drug alone. As depicted in Fig. 5E and Fig. S8, pharmacokinetic analysis revealed that VCit-SN38 (drug only) is rapidly eliminated from the blood, demonstrating a half-life as short as 0.5 h. However, Fab-

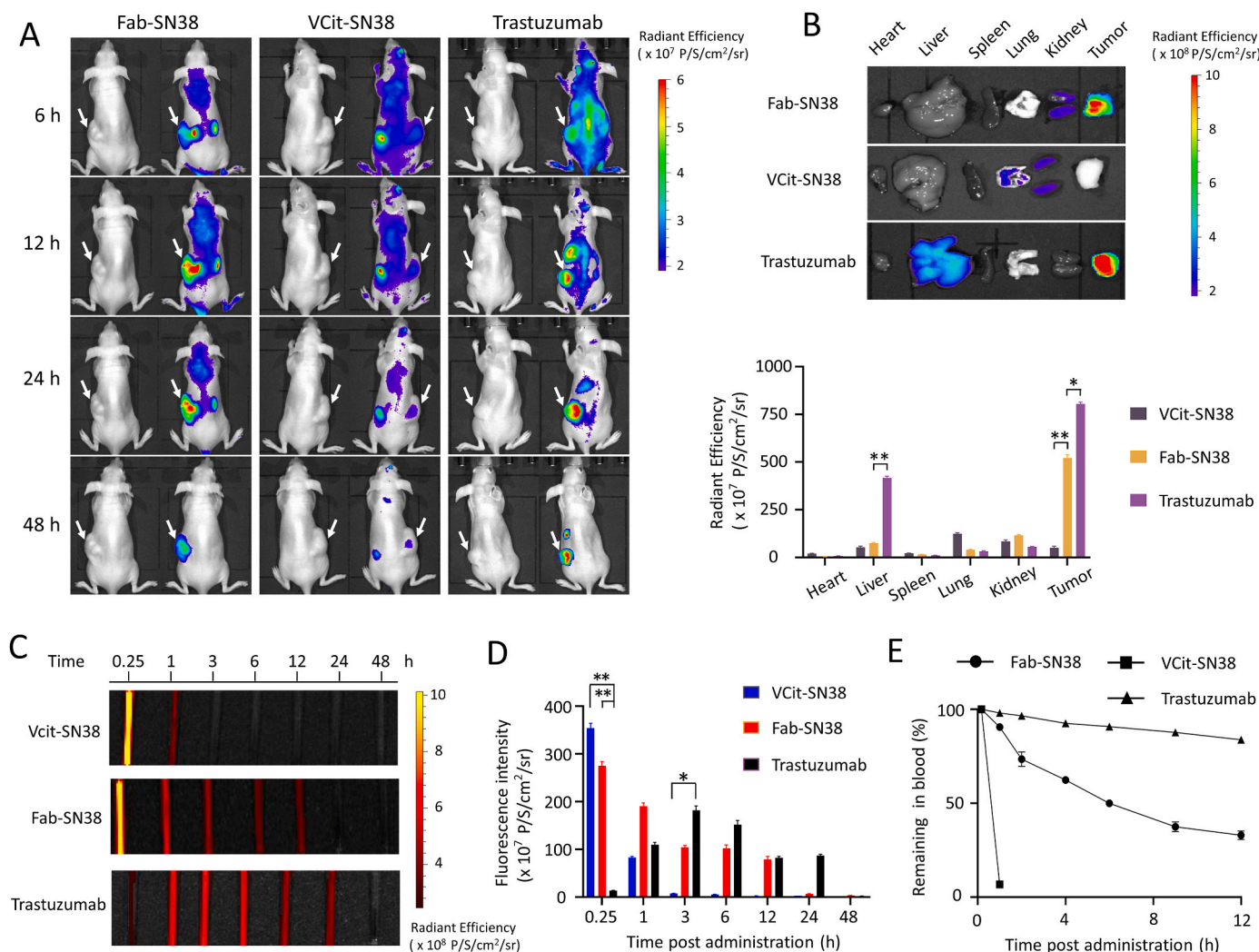


Fig. 5. In vivo biodistribution of the conjugates in mice. (A) In vivo tracking of Fab-SN38, VCit-SN38 and trastuzumab in mice bearing NCI-N87 tumors. Arrows indicate the tumor sites. (B) Fluorescent images of the dissected tissues and tumors at 48 h after IV administration (upper). Quantification analysis of average radiant efficiency in organs was listed below. Data are shown as mean \pm SD ($n = 3$), * $P < 0.05$, ** $P < 0.01$. (C) Urine analysis of the mice treated by sulfo-Cy5 labeled VcIt-SN38, Fab-SN38 or trastuzumab at different time points. (D) Quantification of urine fluorescence in Fig. 5C. Data are shown as mean \pm SD ($n = 3$), * $p < 0.05$, ** $p < 0.01$. (E) Pharmacokinetic profiles of Fab-SN38, VCit-SN38 and trastuzumab after a single IV injection. Data are shown as mean \pm SD ($n = 3$).

SN38 exhibited a circulating half-life of approximately 6 h, with more than 30% remaining even after 12 h. It is worth noting that the blood circulation time of Fab-SN38 is significantly shorter than that of the full-length antibody. However, it is what we expected, because the shorter half-life in vivo increases the animal tolerance to high-dose therapy or multiple injections, which is important to payloads like SN38.

2.7. Therapeutic efficacy in vivo

The antitumor efficacy of Fab-SN38 was evaluated in BALB/c nude mice bearing either NCI-N87 or Calu-3 tumors by tail vein administration. In both groups, the drugs were injected every three days for a total of four doses (7 mg/kg per dose in case of Fab-SN38) after the tumor reached 100 mm³. The dose regimen was scheduled slightly higher per dose and more frequently than the conventional ADCs, for example, 1 mg/kg, single injection for DS-8201a and 0.5 mg weekly, two injections for sacituzumab govitecan in mice [37,38]. Considering the short systemic exposure of Fab-SN38 in mice, an even higher dosage can be applied. Although the Fab-SN38 demonstrated the best therapeutic efficacy in both models, its effect on Calu-3 xenograft was more prominent than that on NCI-N87 (Fig. 6A). The discrimination in efficacy may be explained by two reasons: higher HER2 expression level and superior

sensitivity to SN38 by Calu-3. Notably, the SN38 or anti-HER2 Fab alone also can slow down the growth of tumors as well. This observation is consistent with the in vitro cytotoxicity assay (Fig. 3A and B) and also in agreement with the reports from other groups [39]. Nevertheless, the antitumor effect of Fab and SN38 by covalent conjugation (Fab-SN38) was much more profound than them alone in both tumor models, indicating the advantages of targeted chemotherapy. As shown in Fig. 6A (right panels), the body weights of the mice in the treatment groups remained constant to the controls. No significant weight loss or side effect was observed after four injections, demonstrating good tolerability of this Fab conjugate.

Histochemical analysis was undertaken to determine the drug deposition in tumors two days after administration. Both trastuzumab, Fab-SN38 and VCit-SN38 were labeled by sulfo-Cy5, and their presence in tumor cryosections was examined by laser scanning confocal microscopy (Fig. 6B and Fig. S9). The Cy5 fluorescence was detected in sections of tumors treated by Fab-SN38 and trastuzumab, but not VCit-SN38. Moreover, the Fab-SN38 distribution in tumors is nearly homogenous, with only a small fraction of the tumor untargeted. In contrast, the deposition of trastuzumab in tumor sections displayed as narrow and spatial spots, indicating the poor penetration of full-length antibodies in tissues. Collectively, these results demonstrated that

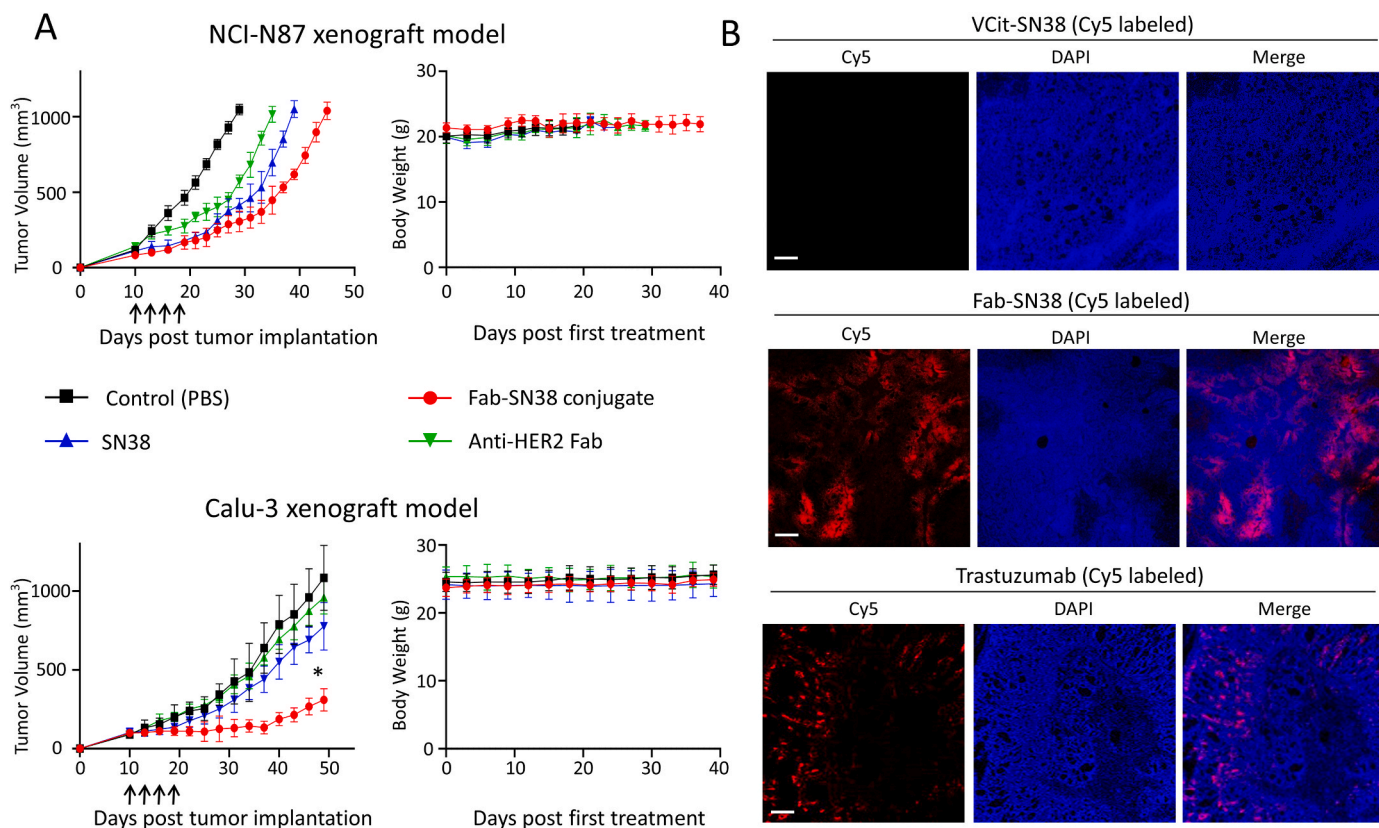


Fig. 6. In vivo antitumor efficacy in mouse xenograft models. (A) The NCI-N87 xenograft mice (upper) and Calu-3 tumor-bearing mice (bottom) were treated by Fab-SN38, Fab, SN38 and PBS control, respectively. All the drugs were administered in an equivalent dose (125 nmol/kg, equal to 7 mg/kg of Fab-SN38) for a total of four doses (arrow indicated). The tumor-growth curves and body-weight curves were listed on left and right, respectively. All data are shown as mean \pm SD (n = 5). *P < 0.05. (B) Confocal imaging of the tumor sections revealed the drug deposition at 48 h after IV administration. Red, Cy5 labeled conjugates; Blue, nucleus counterstained by DAPI. Scar bar, 200 μ m. (For interpretation of the references to color in this figure legend, the reader is referred to the Web version of this article.)

anti-HER2 Fab can deeply penetrate solid tumors.

3. Discussion

Fab drug conjugates have the potential to become a transformative therapy for cancer patients aside of ADCs. This format was first reported in 2007 but has received limited attention to date [17]. One obstacle that impedes progress is the efficient production of Fab protein [21]. Fab possesses two different peptide chains that can fold into 4 domains and 3 pairs of cysteines (2 intrachain and 1 interchain disulfide bonds). Despite much smaller than antibody, Fab remains difficult to express in *E. coli* [40]. The scFab scaffold joins two Fab chains into one by introducing a peptide linker between LC and HC. Thus, it combines some advantages of scFv (for example, single gene and one expression plasmid) with a better stability and lower tendency to aggregate. The proximity effect of the linker also promotes the correct light/heavy chain pairs and the interchain disulfide bond formation, both of which help prevent the ‘devoid of light chain’, a phenomenon commonly seen in Fab expression [27,29,31]. A pilot study of an anti-HER2 scFab carrying a flexible 63aa linker results in the high expression in *E. coli*. To diminish the potential hypersensitivity reaction in therapy, the artificial peptide linker was cleaved from the purified scFab before drug conjugation.

Departure from the common ADCs that utilize ultratoxic chemical drugs, this construct selects the chemotherapeutic agent SN38. It is the therapeutically active metabolite of the anticancer drug irinotecan, with a nanomolar activity against a broad range of cancer cells. SN38 is less potent than most ADC toxins but has a high window of tolerance [41]. In this study, the use of SN38 as the payload for Fab conjugate addressed multiple challenges, which can feature in the following aspects: first, the

γ -carboxyl group of Glu was esterified with the 20-hydroxy position of SN38. The strong steric hindrance minimizes the premature release of SN38 from Fab conjugate. When placed in mouse serum and held at 37 °C, SN38 is released from the conjugate with a half-life of >12 h, which is much longer than its circulation half-life. Secondly, the VCit linker and self-immolative spacer Glu support the traceless release of SN38. The VCit dipeptide linker is a common protease-sensitive linker in ADCs. It always cooperates with a self-immolative *p*-aminobenzyloxy carbamoyl (PABC) spacer to control the release of the amine-containing toxin [42]. Due to the absence of amine group in SN38, we introduced a new immolative linker glutamic acid (Glu). It promotes the γ -ester hydrolysis and SN38 release by a 5-membered ring closure mechanism. We also proved that the ring closure metathesis is pH dependent (Fig. 2C). Thirdly, SN38 was site-specifically grafted on the C-terminus of Fab heavy chain by a sortase A ligation. Rebridging of the native interchain disulfide bond has been the most common strategy to conjugate drugs to Fab [43,44]. However, this approach requires a partial reducing step to break up the interchain disulfide bond before a rebridging conjugation. Because of the weak pairing force between LC and HC (interchain disulfide bond is a much stronger covalent force), this step poses a risk of chain-pair disruption. Without touching the interchain disulfide bond, we utilized a sortase A ligation to produce a stable Fab-SN38 conjugate and achieve a homogenous drug-to-antibody ratio (DAR) of 1. The obtained conjugate also is fully functional in HER2 receptor binding and tumor cell killing.

It is worth noting that each cell line revealed different biological responses to anti-HER2 Fab treatment. Despite the high-level expression of HER2 receptors, Calu-3 and SK-OV-3 were reluctant to the Fab treatment; while it was controversial with NCI-N87 cells (Fig. 3A). Several reports suggested that trastuzumab induced cytostatic effect

(G0/G1 arrest) of NCI-N87 through the HER2/HER3/PI3K pathway, which downregulates AKT activity and inhibits the proliferation [45–47]. However, the trastuzumab-insensitive cell lines, such as Calu-3 and SK-OV-3, carry the hot spot mutation in PIK3CA, thus uncoupling PI3K activity from the HER2/HER3 oncogenic unit and rendering the cells resistant to the Fab treatment [48]. Although HER2 amplification is an important biomarker to predict the treatment outcomes of anti-HER2 drugs, the heterogeneous response poses a challenge to the further validation and potential application of Fab-SN38 conjugate. We hypothesized that the maximal therapeutic benefit would be seen in HER2-positive cancer modes of both trastuzumab-sensitive and SN38-sensitive. Unfortunately, it has not been validated in this study, because most trastuzumab-sensitive cell lines, including many breast cancer cell lines and gastric cancer cell line NCI-N87 in this study, are tolerant to the SN38 treatment ($IC_{50} > 100$ nM). However, we expect a promising therapeutic utilization in HER2-positive patients owing to the diversified pattern of pathology in clinic.

Full-length antibodies can be retained in the bloodstream for a very long time due to the ability of the Fc region to bind with the nascent Fc receptor (FcRn) in a pH-dependent manner [49]. As for ADCs, the extremely long half-life in bloodstream is a two-edged sword, producing a higher delivery efficiency but associating with a toxicity risk due to the long systemic exposure [11]. As a fragment of the antibody, Fab is much smaller in size and can be excreted via renal filtration (Fig. 4C). Notably, this protein is large enough to allow the conjugates remaining in the blood for a period and the time is long enough to deliver the drug to tumors, eventually giving a high tumor-to-blood ratio. The compact size of the drug conjugates is also beneficial to tumor penetration (Fig. 5B), which has been extensively discussed somewhere else [50].

4. Conclusion

In the field of oncology, targeted therapies have received significant attention. HER2 is a crucial target in targeted tumor therapy. The anti-HER2 mAb trastuzumab and its ADC have shown exceptional clinical success in HER2-targeted therapy. In this study, we investigated a trastuzumab fragment-based drug conjugate, anti-HER2 Fab-SN38. By finely tuning the conjugation modality and release mechanism, the conjugate has exhibited excellent specificity and efficacy towards HER2-positive tumor cells both *in vitro* and *in vivo*. This study demonstrated the potentials of the antibody fragment-based drug conjugates in target cancer chemotherapy, which may open up new perspectives for novel drug conjugates using Fabs.

5. Materials and methods

5.1. Materials

SN38 and trastuzumab were purchased from MedChemExpress (MCE, USA). Roswell Park Memorial Institute (RPMI) 1640 Medium, Iscove's Modified Dulbecco's Medium (IMDM), Dulbecco's Modified Eagle Medium (DMEM), Fetal Bovine Serum (FBS), Penicillin-Streptomycin (PS) solution, 0.25% trypsin-EDTA solution were purchased from Gibco (Waltham, USA). The cyanine 5 (sulfo-Cy5) and cyanine 7 (sulfo-Cy7) NHS esters were purchased from Duofluor Inc. (Wuhan, China). Bovine spleen cathepsin B, TEV protease, Cell Counting Kit-8 (CCK-8), bovine serum albumin (BSA) and DBCO-Cy3 were purchased from Sigma Aldrich (St. Louis, USA). Dead Cell Apoptosis Kit with Annexin V Alexa Fluor™ 488 & Propidium Iodide were purchased from Thermo Fisher Scientific (Waltham, USA). Cell Cycle Analysis Kit was purchased from Beyotime Biotechnology (Shanghai, China). Amine Reactive Second-Generation (AR2G) Biosensors and 10X kinetics buffer were purchased from Sartorius (Göttingen, Germany). Recombinant Human HER2/ERBB2 Protein (ECD, His Tag) was purchased from Sino Biological (Beijing, China). All the organic solvents and chemicals were obtained from Macklin Inc. (Shanghai, China).

5.2. Cell culture

The cancer cell lines MDA-MB-231, SK-OV-3, Calu-3, NCI-N87 and Capan-1 were obtained from American Type Culture Collection (ATCC, USA). SK-OV-3, Calu-3, and NCI-N87 cells were cultured in RPMI 1640 medium supplemented with 10% FBS and 1% PS. Capan-1 cells were cultured in IMDM medium supplemented with 20% FBS and 1% PS. MDA-MB-231 cells were cultured in DMEM medium supplemented with 10% FBS and 1% PS. All cells were cultured in a humidified cell culture incubator at 37 °C with 5% CO₂.

5.3. Expression and purification of scFab

The sequences of the anti-HER2 Fab chains were obtained from trastuzumab. Between light chain and heavy chain was inserted by a 63aa peptide linker. It contains two TEV substrate peptide sequence (ENLYFQS) and four 3×His tags. The C-terminus of the scFab was fused with a sortase A substrate peptide sequences (LPETGG). The cDNA of the scFab was synthesized by Sangon Biotech Co. Ltd (Shanghai), and the gene was then cloned in the pET28a(+) expression vector to generate pET-28a/scFab via Gibson assembly. The vector was transformed into BL21(DE3) and the protein expression was induced by the Studier autoinduction method [51]. Bacteria were harvested by centrifugation at 8000 g for 10 min, followed by lysis by French press homogenization. The soluble proteins were collected and the scFab protein was purified by Ni-affinity chromatography. The protein sequence of scFab was shown as follows:

```
MDIQMTQSPSSLSASVGDRTITCRASQDVNTAVA-
WYQQKPGKAPKLLIYSAS-
FLYSGVPSRFRSGSRGTDFTLTISSLQPEDFA-
TYYCQQHYTTPPTFGQGTKVEIKRTVAAPSVFIFPPSDEQLKSG-
TASVVCLLNFFYPREAKVQWKVDNALQSGNSQESVTEQDSKD-
STYLSLSTLTLSKADYEEKHKVYACEVTHQGLSSPVTKSFNRGEC-
SENLYFQSGSGGSGRSGSHHHEGDDHHHGE-
SEGHHHGSRGHHHSGSGSDGGSGSENLYFQSEVQL-
VESGGGLVQPGGSLRLSCAASGFNIKDTYIHWVRQAPGKLEWVAR-
IYPTNGY-
TRYADSVKGRFTISADTSKNTAYLQMNSLAEDTA-
VYYCSRWGGDGFYAMDYWGQGLTVSSASTKGPSVF-
PLAPSSKSTSGGTAALGCLVKDYFPEPVTVSWNSGALTSVHHTF-
PAVLQSS-
GLYSLSSVTVPSSSLGTQTYICNVNHKPSNTKVDKRVKPKSCDKL-
PETGG*
```

5.4. Fab-SN38 preparation

To convert the scFab to Fab, the purified scFab protein (20 mg/mL) was first incubated with the TEV protease at an enzyme-to-target protein ratio of 1:100 at room temperature for 120 min. The protein was then purified using cation exchange chromatography and dissolved in TBS buffer by dialysis. Next, the sortase A-mediated transpeptidation was performed to ligate the C-terminus of the heavy chain with an azide group. Briefly, the Fab protein was diluted to 9 mg/mL in TBS buffer and co-incubated with GGG-PEG3-azide (1 mM) at room temperature overnight in the presence of 200 nM of 7 M sortase A (a calcium-independent sortase A variant with enhanced activities) [52]. The product was precipitated from the reaction using an 85% ammonium sulfate solution and desalted with G25 column (GE Life Sciences). Finally, the purified Fab-azide was coupled with BCN-VCit-SN38 (3 eq) by a copper-free click reaction. The reaction mixture was purified by size exclusion chromatography (Superdex 200 Increase 10/300 GL) to remove any unreacted BCN-VCit-SN38. The final conjugate was stored at -20 °C in the presence of 20% glycerol.

5.5. Bio-layer interferometry (BLI) assay

BLI analysis was performed at 30 °C using a ForteBio Octet Red96e biosensor system (ForteBio, Germany) with Amine Reactive Second-Generation Biosensors. The AR2G biosensors were initially activated with EDC and sulfo-NHS for 15 min. Recombinant Human HER2 ECD protein (20 µg/mL) was immobilized onto the AR2G biosensor for another 10 min. The immobilization reaction was quenched with 1 M ethanolamine for 5 min and the tips were washed with the kinetics buffer for 2 min to obtain a baseline reading. Thereafter, the biosensors were dipped into wells containing the various concentrations of trastuzumab (from 0.1 to 10 nM), scFab protein (from 0.3 to 30 nM) or Fab protein (from 0.3 to 30 nM) for 10 min, which was followed by a 5-min buffer wash to allow the dissociation of molecules from the sensor. The data were analyzed using the ForteBio Data Analysis 11.1 software with a standard 1:1 binding model.

5.6. Chemical synthesis of BCN-VCit-SN38

5.6.1. Synthesis of Boc-SN38 (compound 1)

The synthesis of Boc-SN38 was modified from the previous report [53]. Briefly, SN38 (196.2 mg, 1 eq) and di-*tert*-butyl decarbonate (196.43 mg, 1.8 eq) were dissolved in 5 mL of DCM, followed by the addition of pyridine (982.5 µL). Two hours after stirring at room temperature, the reaction was stopped and washed by aqueous hydrochloric acid solution (0.5 M). The organic phase was dried with Na₂SO₄, and then concentrated under vacuum to give crude Boc-SN38. The residue was purified by silica gel chromatography using DCM/MeOH (v/v, 50/1) as eluant. The pure compound 1 was obtained as a yellow solid (233.95 mg, yield 95%). HR-MS: *m/z* calcd for C₂₇H₂₉N₂O₇ [M + H]⁺ 493.1975, found 493.1969.

5.6.2. Synthesis of compound 2

To synthesize compound 2, Boc-SN38 (233.95 mg, 1 eq) and Z-Glu-OtBu (770.3 mg, 5 eq) were dissolved in DCM, followed by adding EDCI (455.3 mg, 5 eq), DMAP (58 mg, 1 eq) and Et₃N (66 µL, 1 eq). After stirring overnight at room temperature, the reaction mixture was washed by 10% citric acid aqueous solution, saturated brine, then concentrated under vacuum. The residue was purified by silica gel chromatography using DCM/MeOH (v/v, 50/1), yielding a light yellow solid (374.1 mg, yield 97%). HR-MS: *m/z* calcd for C₄₄H₅₀N₃O₁₂ [M + H]⁺ 812.3394, found 812.3379.

5.6.3. Synthesis of compound 3

To remove the Cbz group, compound 2 (374.1 mg, 1 eq) was dissolved in ethyl acetate (15 mL) and 10% Pd/C was added. The reaction was hydrogenated at room temperature and atmospheric pressure for 3 h. Then the catalyst was filtered off through celite, and the clear solution was concentrated. The compound 3 was obtained as a colorless oil (302.9 mg, 97%) and used in the next step without purification. HR-MS: *m/z* calcd for C₃₆H₄₄N₃O₁₀ [M + H]⁺ 678.3027, found 678.3032.

5.6.4. Synthesis of compound 5

The Boc-VCit-OH (compound 4) was purchased from Bidepharm (Shanghai, China). To a stirred solution of compound 4 (111.4 mg, 1 mmol) in DMF, HATU (190.12 mg, 2 mmol) and DIPEA (130 µL, 3 mmol) was added to activate the carboxyl group for 10 min. Then compound 3 (254.2 mg, 1.5 mmol) in DCM was added. The mixture was stirred at room temperature for an additional 2 h and the reaction was quenched with water (1 mL). The reaction mixture was washed with 10% citric acid aqueous solution and the organic phase was dried with Na₂SO₄, then concentrated under a vacuum to give the crude product. The residue was purified by silica gel chromatography using DCM/MeOH (v/v, 30/1), giving the pure compound 5 as a yellow oil (233.95 mg, 85%). HR-MS: *m/z* calcd for C₅₅H₇₇N₈O₁₆ [M + H]⁺ 1105.5458, found 1105.5442.

5.6.5. Synthesis of VCit-SN38 (compound 6)

VCit-SN38 was obtained from compound 5 by removal of the Boc protecting group by treatment with trifluoroacetic acid (TFA). Compound 5 (234.9 mg) was dissolved in a solution of 40% TFA in dichloromethane (10 mL) at room temperature. The reaction progress was monitored by TLC. At the end of the reaction, the mixture was evaporated under reduced pressure. The residue was washed with methyl *tert*-butyl ether, and then purified by silica gel flash column chromatography to give VCit-SN38 (120 mg, 67%) as a light yellow solid. HR-MS: *m/z* calcd for C₄₁H₅₃N₈O₁₂ [M + H]⁺ 849.3783, found 849.3768.

5.6.6. Synthesis of BCN-VCit-SN38 (compound 7)

BCN-NHS (25.7 mg, 2.5 eq) and DIPEA (16 µL, 2.5 eq) were added to the solution of VCit-SN38 (30 mg, 1 eq) in DMF and the mixture was stirred at room temperature. The reaction was monitored by TLC. The mixture was diluted with water and was purified by silica gel flash column chromatography to give BCN-VCit-SN38 (28 mg, 77%) as a light yellow solid. HR-MS: *m/z* calcd for C₅₂H₆₃N₈O₁₄ [M - H]⁺ 1023.4464, found 1023.4460.

5.7. SN38 release assay

For the cathepsin B cleavage assay, the release assay was performed in the assay buffer of 25 mM sodium acetate (pH 5.5, the optimal pH of cathepsin B) in the presence of 1 mM EDTA. The cathepsin B enzyme was first activated at ambient temperature for 15 min using the assay buffer containing 10 mM DTT. The activated cathepsin B was added into a VCit-SN38 solution in the assay buffer to reach a final concentration of 100 nM (cathepsin B) and 125 µM (VCit-SN38). The reaction mixture was then incubated at 37 °C. At the indicated time points (1 h, 2 h, 3 h, 5 h, 7 h), 20 µL of the sample was taken from the solution and immediately quenched by adding 10 µL of acetonitrile. The samples were analyzed by HPLC (gradient method increasing linearly from 5% to 95% solvent B in 30 min, UV detection wavelength of 265 nm) and the molecular mass of major peaks was characterized by high-resolution Orbitrap mass spectrometry (Thermo Fisher, USA).

To verify the release of SN-38, Glu(SN38)-OH was dissolved in PBS solution (pH 7.4) to a final concentration of 200 µM. The mixture was incubated with gentle shaking at 37 °C. The aliquots were collected at 4, 8, 12, 16, 18, and 20 h, and each aliquot was immediately quenched and analyzed by HPLC as described above.

5.8. Stability assay

To evaluate the stability, the compound BCN-VCit-SN38 was dissolved in PBS solution, complete culture media, and mouse plasma at a final concentration of 200 µM, respectively. The solution was incubated at 37 °C with gentle shaking. At the indicated time points (2 h, 4 h, 6 h, 8 h, 10 h, 12 h), 20 µL of the solution was taken out and reconstituted with 10 µL of acetonitrile. The mixtures were analyzed by HPLC (Shimadzu, Japan).

5.9. In vitro cytotoxicity assay

The cytotoxicity of Fab-SN38 was evaluated using the Cell Counting Kit-8 (CCK-8) assay. Cells (MDA-MB-231, Calu-3, NCI-N87 and SK-OV-3 cells) were seeded into clear-bottom 96-well plates (~3000 cells per well). After overnight culture, the medium was removed and the fresh medium containing SN38, Glu(SN38)-OH, Glu-SN38, trastuzumab, the Fab protein or the Fab-SN38 conjugate was added and incubated for 72 h at 37 °C in a CO₂ incubator. Cell viability was measured using the CCK-8 reagent according to the protocol. Briefly, 15 µL of CCK-8 solution was added to the culture media. Two hours after incubation at 37 °C, the absorbance at a wavelength of 450 nm was measured by a microplate reader (TECAN, Switzerland) and then the IC₅₀ value was profiled using

the Graphpad Prism 8 software.

5.10. Apoptosis assay

Cell apoptosis was detected via flow cytometry after staining with Alexa Fluor 488 Annexin V/Propidium Iodide Dead Cell Apoptosis Kit (Thermo Fisher, USA) according to the manufacturer's instructions. Briefly, cells (Calu-3, NCI-N87 and SK-OV-3 cells) were seeded into clear-bottom 6-well plates ($\sim 1 \times 10^5$ cells per well) and allowed to adhere overnight. Subsequently, the medium was replaced with fresh medium (control group) or the medium containing either SN38 (10 nM), the Fab protein (10 $\mu\text{g}/\text{mL}$) or the Fab-SN38 conjugate (10 $\mu\text{g}/\text{mL}$). The cells were incubated for 36 h at 37 °C in a cell culture incubator supplemented with 5% CO₂. Cells were collected and washed with cold PBS for three times and then resuspended in 100 μL of 1 \times annexin-binding buffer. Then, 5 μL of Alexa Fluor 488 Annexin V and 1 μL propidium iodide (PI) working solution (100 $\mu\text{g}/\text{mL}$) were added to each cell suspension. Cells were gently vortexed and incubated for 15 min at RT (25 °C) in the dark. 400 μL of 1 \times annexin-binding buffer was added to each tube before performing flow cytometry. The percentage of apoptotic cells was calculated and analyzed using the FlowJo software.

5.11. Cell cycle analysis

The cell cycle assay was performed using the Cell Cycle Analysis Kit. Cells (Calu-3, NCI-N87 and SK-OV-3 cells) were plated in 12-well culture dishes ($\sim 1 \times 10^6$ cells per well) and allowed to adhere overnight. Subsequently, the medium was replaced with fresh medium (control group) or the medium containing either SN38 (10 nM), the Fab protein (10 $\mu\text{g}/\text{mL}$) or the Fab-SN38 conjugate (10 $\mu\text{g}/\text{mL}$). Cells were incubated for 36 h at 37 °C in a cell culture incubator. The medium was removed, the cells were harvested as suspension, washed twice with cold PBS, and fixed in 70% ethanol for 4 h at 4 °C separately. The suspensions were then centrifuged at 800 g for 5 min, washed with cold PBS and incubated with PI staining solution containing RNase A at 37 °C for 30 min in the dark according to the protocol. Samples were then analyzed and DNA content was determined by flow cytometry (Beckman, USA). Flow cytometric data were analyzed using the FlowJo software.

5.12. Cell binding and flow cytometry analysis

Flow cytometry was used to analyze and compare the binding selectivity of Fab-SN38 to the HER2 receptors on cell membranes. The sulfo-Cy5 NHS ester was reacted with amino groups of Fab-SN38 according to the manufacturer's recommendation. The labeled product was then purified by desalting on Sephadex G25 column (Cytiva, USA). To titrate the concentration-dependent binding, a series concentration of sulfo-Cy5 labeled Fab-SN38 (from 1 nM to 300 nM, dye quantification) were incubated separately with the cells (~ 20000 cells) in RPMI 1640 medium supplemented with 1% BSA for 1 h at room temperature. Cells were washed twice with DPBS and resuspended in serum-free RPMI 1640 medium and analyzed the Cy5 intensity using a BD LSR II flow cytometer (Beckton Dickinson). To profile the binding on different cell types, sulfo-Cy5 labeled Fab-SN38 (100 nM, Cy5 equivalent) was incubated with various cancer cells (~ 20000 cells, MDA-MB-231, SK-OV-3, Calu-3, and NCI-N87 cells) in RPMI 1640 medium supplemented with 1% BSA for 1 h at room temperature. The cell binding was then analyzed by flow cytometry as described above.

5.13. Western blotting analysis

Cells (MDA-MB-231, SK-OV-3, Calu-3, NCI-N87, and Capan-1 cells) were cultured in the cell culture dish. When reaching 80% confluence, cell monolayers were scraped with cell scrapers, washed twice with PBS, and lysed for 15 min on ice with IP lysis buffer (Thermo Fisher) supplemented with protease inhibitors (Roche's complete protease

inhibitor cocktail tablet). The lysates were centrifuged at 12,000g for 10 min. The supernatant was then collected and the total protein concentration of each sample was measured by BCA assay. 20 μg of each cell lysate was separated on a 12% SDS-PAGE gel and transferred to a polyvinylidene difluoride (PVDF) membrane. The membrane was blocked for 2 h in TBST buffer supplemented with 1% BSA. The membrane was then incubated with a primary antibody (polyclonal rabbit anti-HER2, Catalog# A21248 or mouse beta-actin, Catalog# AC004, ABclonal, China) overnight at 4 °C. After three rinses with TBST, the membrane was incubated for 2 h with a horseradish peroxidase (HRP)-linked secondary antibody (goat anti-rabbit IgG, goat anti-mouse IgG, Invitrogen, Grand Island, NY). After washing with the TBST buffer, the membrane was incubated with Western Detection Kit (Cell Signaling Technologies, USA) and the bands were imaged by ChemiDoc Imaging Systems (Bio-Rad, USA).

5.14. Cellular uptake assay

Confocal laser scanning microscopy was used to track the sulfo-Cy5 labeled Fab-SN38 in cancer cells. SK-OV-3 cells (~ 50000 cells) were seeded in a confocal dish one day before experiments. Cell monolayer was washed with DPBS and incubated with sulfo-Cy5 labeled Fab-SN38 in RPMI-1640 medium at 37 °C. The cells were incubated with Fab-SN38 at a final concentration of 8 μM (SN38 equivalent). It is noted that a relatively high concentration is required to directly track the SN38 due to its relatively faint fluorescence of SN38. Cells were imaged by confocal laser scanning microscopy (Leica, USA) at the indicated time points (30 min, 2 h, 4 h). The fluorescent signal of both Cy5 (ex/em 649/672 nm) and SN38 (ex/em 377/556 nm) were collected.

5.15. In vivo biodistribution

All animal experiments were performed in accordance with the guidelines of the Chinese Regulations for the Administration of Affairs Concerning Experimental Animals and the Institutional Animal Care and Use Committee of Wuhan University. NCI-N87 cells ($\sim 5 \times 10^6$ cells) were suspended in a 1:1 mixture of RPMI 1640 (Gibco) and Matrigel (Corning, USA), and then subcutaneously implanted into the dorsal region of female BALB/c-nu mice (6–8 weeks old). Tumor growth was measured every 3 days and the size was calculated using the formula length \times width²/2. The biodistribution study was performed when the tumor volume reached 400–600 mm³. The mice were injected with either sulfo-Cy5 labeled Fab-SN38 (5 mg/kg) or sulfo-Cy5 labeled VCit-SN38 (equal dye dose) or sulfo-Cy5 labeled trastuzumab (equal dye dose) via the tail vein. The biodistribution of drugs was then imaged using the IVIS Lumina III imaging system (Caliper, USA) at 6, 12, 24, and 48 h. At the end of the experiment, the mice were sacrificed. The dissected tumors and major organs, including heart, lung, liver, spleen, and kidney, were collected and imaged. For urine analysis, the mouse urine was collected in glass capillary tube at indicated time points and imaged using the IVIS Lumina III system. The dissected tumors were then frozen for section analysis. The tumor specimens were sectioned into 15 μm slices and stained with 4',6-diamidino-2-phenylindole (DAPI), which is commonly used for nucleus counterstaining. The distribution of Cy5 labeled drugs in sections was imaged by the laser confocal microscopy (Leica, USA).

5.16. Pharmacokinetic study

Fab-SN38, VCit-SN38 and trastuzumab were labeled by sulfo-Cy7 NHS esters according to the manufacturer's protocol (Duofluor, Inc.). BALB/c mice were intravenously injected with either sulfo-Cy7 labeled Fab-SN38 (5 mg/kg) or sulfo-Cy7 labeled VCit-SN38 (equal dye dose) or sulfo-Cy7 labeled trastuzumab (equal dye dose). Blood (20 μL) was collected at 10min, 1, 2, 4, 6, 9, 12 h post-injection. The samples were immediately mixed with heparin to avoid coagulation. The samples

were imaged and quantified using an Odyssey CLx imaging system (LI-COR Biosciences, USA).

5.17. *In vivo* efficacy studies

NCI-N87 or Calu-3 cells were implanted into the female BALB/c-nu mice as described above. When tumor sizes reached 100 mm³, mice were divided into four groups (n = 5). Fab-SN38, Fab protein, SN38 or PBS were administered intravenously through the tail vein with a dose regimen of every 3 days for a total of four doses. Fab-SN38 was given at a dose of 7 mg/kg per injection. The Fab protein and SN38 were administered in equivalent amounts to either Fab or SN38 of the Fab-SN38 conjugate. Body weights and tumor sizes were measured every 3 days. Mice were euthanized when the tumor sizes exceeded 1000 mm³. The tumor growth curves were plotted in GraphPad Prism 8 (GraphPad, USA).

5.18. Statistical analysis

The mean ± standard deviation (SD) was used to report all data. A GraphPad Prism software was used to conduct statistical comparisons using the student's *t*-test as **P* < 0.05, ***P* < 0.01. A difference of **P* < 0.05 was considered significant.

CRedit authorship contribution statement

Ruolin Xu: Writing – original draft, Validation, Methodology, Investigation. **Yan Zheng:** Visualization, Methodology, Formal analysis. **Wanyi Tai:** Writing – review & editing, Supervision, Formal analysis, Conceptualization.

Declaration of competing interest

The authors declare that they have no known competing financial interests or personal relationships that could have appeared to influence the work reported in this paper.

Data availability

Data will be made available on request.

Acknowledgement

This work was financially supported by the National Key R&D Program of China (Grant No. 2021YFA0909900) and the National Natural Science Foundation of China (Grant No. 82073770 and 82273860).

Appendix A. Supplementary data

Supplementary data to this article can be found online at <https://doi.org/10.1016/j.biomaterials.2024.122798>.

References

- J.M. Sasso, R. Tenchov, R. Bird, K.A. Iyer, K. Ralhan, Y. Rodriguez, Q.A. Zhou, The evolving landscape of antibody-drug conjugates: in depth analysis of recent research progress, *Bioconjugate Chem.* 34 (11) (2023) 1951–2000.
- Z. Fu, S. Li, S. Han, C. Shi, Y. Zhang, Antibody drug conjugate: the "biological missile" for targeted cancer therapy, *Signal Transduct. Targeted Ther.* 7 (1) (2022) 93.
- C. Dumontet, J.M. Reichert, P.D. Senter, J.M. Lambert, A. Beck, Antibody-drug conjugates come of age in oncology, *Nat. Rev. Drug Discov.* 22 (8) (2023) 641–661.
- A.Q. Dean, S. Luo, J.D. Twomey, B. Zhang, Targeting cancer with antibody-drug conjugates: promises and challenges, *mAbs* 13 (1) (2021) 1951427.
- R. Colombo, J.R. Rich, The therapeutic window of antibody drug conjugates: a dogma in need of revision, *Cancer Cell* 40 (11) (2022) 1255–1263.
- M.Z. Liao, D. Lu, M. Kågedal, D. Miles, D. Samineni, S.N. Liu, C. Li, Model-informed therapeutic dose optimization strategies for antibody-drug conjugates in oncology: what can we learn from US food and drug administration-approved antibody-drug conjugates? *Clin. Pharmacol. Therapeut.* 110 (5) (2021) 1216–1230.
- G. Lu, N. Nishio, N.S. van den Berg, B.A. Martin, S. Fakurnejad, S. van Keulen, A. D. Colevas, G.M. Thurber, E.L. Rosenthal, Co-administered antibody improves penetration of antibody-dye conjugate into human cancers with implications for antibody-drug conjugates, *Nat. Commun.* 11 (1) (2020) 5667.
- H. Uppal, E. Doudement, K. Mahapatra, W.C. Darbonne, D. Bumbaca, B.Q. Shen, X. Du, O. Saad, K. Bowles, S. Olsen, G.D. Lewis Phillips, D. Hartley, M. X. Sliwkowski, S. Girish, D. Dambach, V. Ramakrishnan, Potential mechanisms for thrombocytopenia development with trastuzumab emtansine (T-DM1), *Clin. Cancer Res. : an official journal of the American Association for Cancer Research* 21 (1) (2015) 123–133.
- M. Aoyama, M. Tada, H. Yokoo, Y. Demizu, A. Ishii-Watabe, Fcy receptor-dependent internalization and off-target cytotoxicity of antibody-drug conjugate aggregates, *Pharmaceut. Res.* 39 (1) (2022) 89–103.
- K. Tsuchikama, Y. Anami, S.Y.Y. Ha, C.M. Yamazaki, Exploring the next generation of antibody-drug conjugates, *Nat. Rev. Clin. Oncol.* 21 (3) (2024) 203–223.
- P. Tarantino, B. Ricciuti, S.M. Pradhan, S.M. Tolane, Optimizing the safety of antibody-drug conjugates for patients with solid tumours, *Nat. Rev. Clin. Oncol.* 20 (8) (2023) 558–576.
- J.C. Masters, D.J. Nickens, D. Xuan, R.L. Shazer, M. Amantea, Clinical toxicity of antibody drug conjugates: a meta-analysis of payloads, *Invest. N. Drugs* 36 (1) (2018) 121–135.
- P.K. Mahalingaiah, R. Ciurlionis, K.R. Durbin, R.L. Yeager, B.K. Philip, B. Bawa, S. R. Mantena, B.P. Enright, M.J. Liguori, T.R. Van Vleet, Potential mechanisms of target-independent uptake and toxicity of antibody-drug conjugates, *Pharmacol. Therapeut.* 200 (2019) 110–125.
- H. Donaghy, Effects of antibody, drug and linker on the preclinical and clinical toxicities of antibody-drug conjugates, *mAbs* 8 (4) (2016) 659–671.
- D.A. Richards, Exploring alternative antibody scaffolds: antibody fragments and antibody mimics for targeted drug delivery, *Drug discovery today, Technologies* 30 (2018) 35–46.
- Z. Li, B.F. Krippendorff, D.K. Shah, Influence of Molecular size on the clearance of antibody fragments, *Pharmaceut. Res.* 34 (10) (2017) 2131–2141.
- X. Wang, J. Zhu, P. Zhao, Y. Jiao, N. Xu, T. Grabinski, C. Liu, C.K. Miranti, T. Fu, B. B. Cao, In vitro efficacy of immuno-chemotherapy with anti-EGFR human Fab-Taxol conjugate on A431 epidermoid carcinoma cells, *Cancer Biol. Ther.* 6 (6) (2007) 980–987.
- X. Chen, G. Ding, Q. Gao, J. Sun, Q. Zhang, L. Du, Z. Qiu, C. Wang, F. Zheng, B. Sun, J. Ni, Z. Feng, J. Zhu, A human anti-c-Met Fab fragment conjugated with doxorubicin as targeted chemotherapy for hepatocellular carcinoma, *PLoS One* 8 (5) (2013) e63093.
- A. Kulmala, T. Huovinen, U. Lamminmäki, Improvement of Fab expression by screening combinatorial synonymous signal sequence libraries, *Microb. Cell Factories* 18 (1) (2019) 157.
- A. Wicki, R. Ritschard, U. Loesch, S. Deuster, C. Rochlitz, C. Mamot, Large-scale manufacturing of GMP-compliant anti-EGFR targeted nanocarriers: production of doxorubicin-loaded anti-EGFR-immunoliposomes for a first-in-man clinical trial, *Int. J. Pharm.* 484 (1–2) (2015) 8–15.
- Z. Zhou, J. Zhang, Y. Zhang, G. Ma, Z. Su, Specific conjugation of the hinge region for homogeneous preparation of antibody fragment-drug conjugate: a case study for doxorubicin-PEG-anti-CD20 Fab' synthesis, *Bioconjugate Chem.* 27 (1) (2016) 238–246.
- Y. Zhao, L. Gutshall, H. Jiang, A. Baker, E. Beil, G. Obmolova, J. Carton, S. Taudte, B. Amegadzie, Two routes for production and purification of Fab fragments in biopharmaceutical discovery research: papain digestion of mAb and transient expression in mammalian cells, *Protein Expr. Purif.* 67 (2) (2009) 182–189.
- R. Rouet, D. Lowe, K. Dudgeon, B. Roome, P. Schofield, D. Langley, J. Andrews, P. Whitfield, L. Jermutus, D. Christ, Expression of high-affinity human antibody fragments in bacteria, *Nat. Protoc.* 7 (2) (2012) 364–373.
- S. Vazulka, M. Schiavinato, M. Wagenknecht, M. Cserjan-Puschmann, G. Striedner, Interaction of periplasmic Fab production and intracellular redox balance in *Escherichia coli* affects product yield, *ACS Synth. Biol.* 11 (2) (2022) 820–834.
- E. Rodríguez-Carmona, O. Cano-Garrido, M. Dragosits, M. Maurer, A. Mader, R. Kunert, D. Mattanovich, A. Villaverde, F. Vázquez, Recombinant Fab expression and secretion in *Escherichia coli* continuous culture at medium cell densities: influence of temperature, *Process Biochem.* 47 (3) (2012) 446–452.
- M. Venturi, C. Seifert, C. Hunte, High level production of functional antibody Fab fragments in an oxidizing bacterial cytoplasm, *J. Mol. Biol.* 315 (1) (2002) 1–8.
- S. Corisdeo, B. Wang, Functional expression and display of an antibody Fab fragment in *Escherichia coli*: study of vector designs and culture conditions, *Protein Expr. Purif.* 34 (2) (2004) 270–279.
- S. Lange, J. Schmitt, R.D. Schmid, High-yield expression of the recombinant, atrazine-specific Fab fragment K411B by the methylophilic yeast *Pichia pastoris*, *J. Immunol. Methods* 255 (1–2) (2001) 103–114.
- K. Mori, H. Hamada, T. Ogawa, Y. Ohmuro-Matsuyama, T. Katsuda, H. Yamaji, Efficient production of antibody Fab fragment by transient gene expression in insect cells, *J. Biosci. Bioeng.* 124 (2) (2017) 221–226.
- T. Furuta, T. Ogawa, T. Katsuda, I. Fujii, H. Yamaji, Efficient production of an antibody Fab fragment using the baculovirus-insect cell system, *J. Biosci. Bioeng.* 110 (5) (2010) 577–581.
- G. Yusakul, S. Sakamoto, H. Tanaka, S. Morimoto, Improvement of heavy and light chain assembly by modification of heavy chain constant region 1 (CH1): application for the construction of an anti-paclitaxel fragment antigen-binding (Fab) antibody, *J. Biotechnol.* 288 (2018) 41–47.

- [32] J.T. Koerber, M.J. Hornsby, J.A. Wells, An improved single-chain Fab platform for efficient display and recombinant expression, *J. Mol. Biol.* 427 (2) (2015) 576–586.
- [33] O. Mijanović, A. Branković, A.N. Panin, S. Savchuk, P. Timashev, I. Ulasov, M. S. Lesniak, Cathepsin B: a sellsword of cancer progression, *Cancer Lett.* 449 (2019) 207–214.
- [34] D.M. Goldenberg, T.M. Cardillo, S.V. Govindan, E.A. Rossi, R.M. Sharkey, Trop-2 is a novel target for solid cancer therapy with sacituzumab govitecan (IMMU-132), an antibody-drug conjugate (ADC), *Oncotarget* 6 (26) (2015) 22496–22512.
- [35] T.M. Cardillo, S.V. Govindan, R.M. Sharkey, P. Trisal, D.M. Goldenberg, Humanized anti-Trop-2 IgG-SN-38 conjugate for effective treatment of diverse epithelial cancers: preclinical studies in human cancer xenograft models and monkeys, *Clin. Cancer Res. : an official journal of the American Association for Cancer Research* 17 (10) (2011) 3157–3169.
- [36] W. Tai, R. Mo, Y. Lu, T. Jiang, Z. Gu, Folding graft copolymer with pendant drug segments for co-delivery of anticancer drugs, *Biomaterials* 35 (25) (2014) 7194–7203.
- [37] T.M. Cardillo, S.V. Govindan, R.M. Sharkey, P. Trisal, R. Arrojo, D. Liu, E.A. Rossi, C.H. Chang, D.M. Goldenberg, Sacituzumab govitecan (IMMU-132), an anti-trop-2/SN-38 antibody-drug conjugate: characterization and efficacy in pancreatic, gastric, and other cancers, *Bioconjugate Chem.* 26 (5) (2015) 919–931.
- [38] Y. Ogitani, T. Aida, K. Hagihara, J. Yamaguchi, C. Ishii, N. Harada, M. Soma, H. Okamoto, M. Oitate, S. Arakawa, T. Hirai, R. Atsumi, T. Nakada, I. Hayakawa, Y. Abe, T. Agatsuma, DS-8201a, A novel HER2-targeting ADC with a novel DNA topoisomerase I inhibitor, demonstrates a promising antitumor efficacy with differentiation from T-DM1, *Clin. Cancer Res. : an official journal of the American Association for Cancer Research* 22 (20) (2016) 5097–5108.
- [39] B. Weigelt, A.T. Lo, C.C. Park, J.W. Gray, M.J. Bissell, HER2 signaling pathway activation and response of breast cancer cells to HER2-targeting agents is dependent strongly on the 3D microenvironment, *Breast Cancer Res. Treat.* 122 (1) (2010) 35–43.
- [40] M. Luo, M. Zhao, C. Cagliero, H. Jiang, Y. Xie, J. Zhu, H. Yang, M. Zhang, Y. Zheng, Y. Yuan, Z. Du, H. Lu, A general platform for efficient extracellular expression and purification of Fab from *Escherichia coli*, *Appl. Microbiol. Biotechnol.* 103 (8) (2019) 3341–3353.
- [41] P. Sapra, H. Zhao, M. Mehlig, J. Malaby, P. Kraft, C. Longley, L.M. Greenberger, I. D. Horak, Novel delivery of SN38 markedly inhibits tumor growth in xenografts, including a camptothecin-11-refractory model, *Clin. Cancer Res. : an official journal of the American Association for Cancer Research* 14 (6) (2008) 1888–1896.
- [42] J.D. Bargh, A. Isidro-Llobet, J.S. Parker, D.R. Spring, Cleavable linkers in antibody-drug conjugates, *Chem. Soc. Rev.* 48 (16) (2019) 4361–4374.
- [43] G. Badescu, P. Bryant, M. Bird, K. Henseleit, J. Swierkosz, V. Parekh, R. Tommasi, E. Pawlisz, K. Jurlewicz, M. Farys, N. Camper, X. Sheng, M. Fisher, R. Grygorash, A. Kyle, A. Abhilash, M. Frigerio, J. Edwards, A. Godwin, Bridging disulfides for stable and defined antibody drug conjugates, *Bioconjugate Chem.* 25 (6) (2014) 1124–1136.
- [44] B.T. Ruddle, R. Fleming, H. Wu, C. Gao, N. Dimasi, Characterization of disulfide bond rebridged fab-drug conjugates prepared using a dual maleimide pyrrolbenzodiazepine cytotoxic payload, *ChemMedChem* 14 (12) (2019) 1185–1195.
- [45] T.T. Junttila, R.W. Akita, K. Parsons, C. Fields, G.D. Lewis Phillips, L.S. Friedman, D. Sampath, M.X. Sliwkowski, Ligand-independent HER2/HER3/PI3K complex is disrupted by trastuzumab and is effectively inhibited by the PI3K inhibitor GDC-0941, *Cancer Cell* 15 (5) (2009) 429–440.
- [46] P. Grell, P. Fabian, M. Khoylou, L. Radova, O. Slaby, R. Hrstka, R. Vyzula, M. Hajdich, M. Svoboda, Akt expression and compartmentalization in prediction of clinical outcome in HER2-positive metastatic breast cancer patients treated with trastuzumab, *Int. J. Oncol.* 41 (4) (2012) 1204–1212.
- [47] A. Ruiz-Saenz, C. Dreyer, M.R. Campbell, V. Steri, N. Gulizia, M.M. Moasser, HER2 amplification in tumors activates PI3K/akt signaling independent of HER3, *Cancer Res.* 78 (13) (2018) 3645–3658.
- [48] A. Chakrabarty, N.E. Bhola, C. Sutton, R. Ghosh, M.G. Kuba, B. Dave, J.C. Chang, C. L. Arteaga, Trastuzumab-resistant cells rely on a HER2-PI3K-FoxO-survivin axis and are sensitive to PI3K inhibitors, *Cancer Res.* 73 (3) (2013) 1190–1200.
- [49] C.H. Lee, T.H. Kang, O. Godon, M. Watanabe, G. Delidakis, C.M. Gillis, D. Sterlin, D. Hardy, M. Cogné, L.E. Macdonald, A.J. Murphy, N. Tu, J. Lee, J.R. McDaniel, E. Makowski, P.M. Tessier, A.S. Meyer, P. Bruhns, G. Georgiou, An engineered human Fc domain that behaves like a pH-toggle switch for ultra-long circulation persistence, *Nat. Commun.* 10 (1) (2019) 5031.
- [50] M.P. Deonarain, Q. Xue, Tackling solid tumour therapy with small-format drug conjugates, *Antibody therapeutics* 3 (4) (2020) 237–245.
- [51] F.W. Studier, Protein production by auto-induction in high density shaking cultures, *Protein Expr. Purif.* 41 (1) (2005) 207–234.
- [52] Q. Wu, H.L. Ploegh, M.C. Truttmann, Hepta-mutant *Staphylococcus aureus* sortase A (SrtA(7m)) as a tool for in vivo protein labeling in *Caenorhabditis elegans*, *ACS Chem. Biol.* 12 (3) (2017) 664–673.
- [53] H. Zhao, B. Rubio, P. Sapra, D. Wu, P. Reddy, P. Sai, A. Martinez, Y. Gao, Y. Lozanguiez, C. Longley, L.M. Greenberger, I.D. Horak, Novel prodrugs of SN38 using multiarm poly(ethylene glycol) linkers, *Bioconjugate Chem.* 19 (4) (2008) 849–859.